**Geomechanics and Engineering**, *Vol. 38, No. 3 (2024) 275-284*
https://doi.org/10.12989/gae.2024.38.3.275


# Evolution of pullout behavior of geocell embedded in sandy soil

Yang Zhao[1,2], Zheng Lu[*1,3], Jie Liu[**2], Jingbo Zhang[4], Chuxuan Tang[1,5] and Hailin Yao[1]

[1]*State Key Laboratory of Geomechanics and Geotechnical Engineering, Institute of Rock and Soil Mechanics, Chinese Academy of Sciences, Wuhan 430071, China*
[2]*Xinjiang Transportation Planning Survey and Design Institute Co., Ltd., Urumqi 830006, China*
[3]*Hubei Key Laboratory of Geo-Environmental Engineering, Wuhan 430071, China*
[4]*CCCC Second Highway Consultants Co., Ltd., Wuhan, 430056, China*
[5]*University of Chinese Academy of Sciences, Beijing 100049, China*

(*Received April 17, 2023, Revised June 25, 2024, Accepted July 18, 20242*)

**Abstract.** This paper aims to explore the evolution of the pullout behavior of geocell reinforcement insights from three-dimensional numerical studies. Initially, a developed model was validated with the model test results. The horizontal displacement of geocells and infill sand and the passive resistance transmission in the geocell layer were analyzed deeply to explore the evolution of geocell pullout behavior. The results reveal that the pullout behavior of geocell reinforcement is the pattern of progressive deformation. The geocell pockets are gradually mobilized to resist the pullout force. The vertical walls provide passive pressure, which is the main contributor to the pullout force. Hence, even if the frontal displacement (FD) is up to 90m mm, only half of the pockets are mobilized. Furthermore, the parametric studies, orthogonal analysis, and the building of the predicted model were also carried out to quantitative the geocell pullout behavior. The weights of influencing factors were ranked. Ones can calculate the pullout force accurately by inputting the aspect ratio, geocell modulus, embedded length, frontal displacement, and normal stress.

**Keywords:** geocells; geosynthetics; predicted mode; pullout resistance

## 1. Introduction

Geocells are special three-dimensional geosynthetics that have been widely applied in subgrade (Zhao *et al.* 2023, Halder and Chakraborty 2020, Khorsandiardebili and Ghazavi 2021, Ardakani and Namaei 2021, Saride *et al.* 2013, Biswas and Mittal 2017, Khalaj *et al.* 2015, Luo *et al.* 2021, Luo *et al.* 2023), and unpaved roads (Yang *et al.* 2013, Yang *et al.* 2012), owing to their excellent performance and cost-effectiveness. The vertical walls of geocells provide lateral confinement and enhance the stiffness and shear strength of granular infill material (Zhao *et al.* 2024a, Zhao *et al.* 2024b). This can be quantified as a drastic improvement in apparent cohesion (Bathurst and Karpurapu 1993, Altay *et al.* 2021, Tafreshi *et al.* 2018, Kumar *et al.* 2019), the most significant advantage compared with other planar geosynthetics. Hence, intuitively and sensually speaking, one believes that the anti-pullout load of geocell reinforcement in embankment stability is usually higher than in the case of geogrid or other 2D geosynthetics. The passive pressure provided by vertical walls is superior to the interface resistance between geogrid and adjacent soil.

In practice, geosynthetics are widely used to reinforce embankments, where the geosynthetics can provide the anti-pullout effect to make the structure more stable (Latha 2011, Saikia and Dash 2024, Wijerathna and Liyanapathirana 2020, Lu *et al.* 2020, Girout *et al.* 2018). For the 2D geosynthetics, many researchers conducted experimental and numerical methods to study the geosynthetics-soil interaction and pullout behavior (Derksen *et al.* 2021, Ren *et al.* 2022, Wang *et al.* 2016, Moraci and Recalcati 2006, Mosallanezhad *et al.* 2016, Karnamprabhakara and Balunaini 2021, Mirzaeifar *et al.* 2022, Mukherjee *et al.* 2021, Pant and Ramana 2022).

These studies proved the influence of various factors on the geogrid response under the pullout force, especially for the interface. The plane geosynthetics can resist the pullout load based on the transverse members, surface roughness, etc. However, few researchers pay attention to the pullout resistance of geocells. Khedkar and Mandal (2009), Isik and Gurbuz (2020), Isik *et al.* (2022), Han *et al.* (2013) conducted a series of tests to study the pullout behavior of geocell reinforcement in cohesionless soil. In these studies, geocells presented a square shape, where the length of the geocell pockets was perpendicular or parallel to the pullout direction. The walls along the longitudinal direction can provide the interface friction, while the walls along the transverse direction provide the passive resistance pressure. The users can separate the total pullout force into two parts (Isik and Gurbuz 2020). However, the placement form differs from the embedded geocell in site engineering. Namaei-kohal *et al.* (2022), Fakharian and Pilban (2021) adopted the diamond-shaped geocells to study the pullout behavior of geocell reinforcement. The effects of

*Corresponding author, Professor
E-mail: zlu@whrsm.ac.cn
**Corresponding author, Senior Engineer
E-mail: hfutliujie@163.com



ISSN: 2005-307X (Print), 2092-6219 (Online)

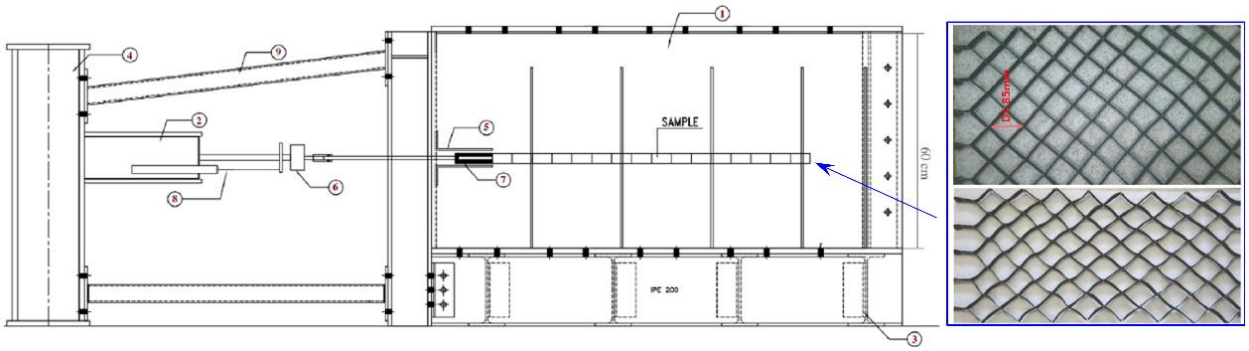


Fig. 1 Schematic view of the longitudinal section of the pullout apparatus (modified from Fakharian and Pilban (2021))

improvements on load-deformation response, strength, and stiffness were investigated in the literature. The mechanism of load transmission was also deeply investigated by comparing it to the pullout behavior of geogrid reinforcement. These studies about the geocell pullout behavior almost discuss the load-deformation response, sum the improvement of geocells, and lack a vivid description of the evolution of pullout behavior. In addition, due to the limitation of experiments (too few experiments), these results can not show the effect of reinforced parameters on the resistance of geocell pullout.

In this context, a study was carried out to explore the evolution of geocell pullout behavior based on the technology of numerical simulations. Primarily, the response of pullout force vs. frontal displacement (FD) was compared from the numerical and experimental results. Also, based on the validated model, the evolution and mechanism for geocell pullout behavior were derived. A series of parametric studies and a sensitivity analysis were conducted to study the tendency and degree of influence. In addition, a regression model was proposed to predict the pullout load by considering the aspect ratio, geocell modulus, embedded length, frontal displacement, and normal stress.

## 2. Experimental background

The pullout tests of geocell-reinforced sandy soil conducted by Fakharian and Pilban (2021) were cited to validate the numerical model (see Fig. 1). The dimensions of the pullout box were 0.6 m × 0.6 m ×1.2 m to eliminate the boundary effect. The inside reinforced soil kept the same length and width as the steel tank, while the height of soil thickness was 0.5 m to leave a 0.1 m space to provide a uniformly distributed normal stress. A medium density of 45% was adopted to easily capture the peak strength and post-peak response. The friction between soil and longitudinal sides was reduced using the polyacrylic plexiglass plates. The geocell was set in the middle of the reinforced soil layer. The soil thickness above and beneath the geocell was 0.25 m. A sleeve (55 mm height and 200 depth) was inserted on the front of geosynthetics to insert a clamp inside the box. A displacement-controlled frontal pullout force was induced at a rate of 1mm/min until one of the following was reached: a) tensile failure of reinforcement, b) pullout failure, or c) displacement reached 92 mm. Also, only the conventional geocells, excluding the diagonally enhanced geocells, were simulated in this study. Table 1 presents the physical and mechanical parameters of sandy soil and geosynthetics.

Table 1 Experimental parameters of sand and geocell (cited from Fakharian and Pilban (2021))

| Crushed silica sand | |
|---|---|
| Relative density, % | 45 |
| Particle size, mm | 0.08~5<br>$D_{50}$=1.15 |
| Diamond geocells | |
| Polymer | Polypropylene |
| Size, mm | Dimension=60<br>Diameter=85<br>Height=25 |
| Thickness, mm | 1.5 |
| Ultimate tensile strength, kN/m | 61.0 |

## 3. Numerical modeling

In this study, the numerical simulations were carried out using finite difference software, Fast Lagrangian Analysis of Continua in Three Dimensions (FLAC$^{3D}$). The full-dimension numerical model was built as 0.6 m × 0.5 m ×1.2 m, in which the steel box was omitted to accelerate the calculation velocity. The null zones, representing the sleeve, were created to keep the same as the model test. Before conducting the numerical simulations, the sensitivity analysis had already been performed to eliminate the influence of mesh size on the numerical results. In this study, the pullout force was decreased with the increase of the mesh numbers, in which the calculated pullout force remains almost constant when the number of zones exceeds 40000. Therefore, excluding the geocell model, the soil model was discretized into 409868 zones in this present study. Diamond-shaped geocell was simulated by the geogrid structural elements. The dimensions of the geosynthetics specimens are 425 mm in width and 720 mm in length. Plus, a single geocell pocket is 60 mm in dimension, 85 mm in diameter, and 25 mm in height. There

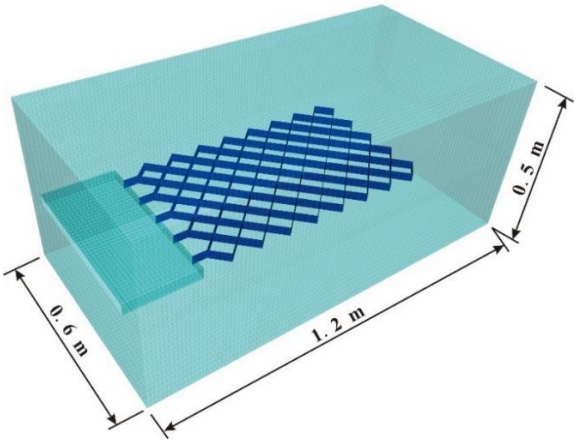


Fig. 2 The numerical model of the geocell pullout test in FLAC$^{3D}$

are two methods to build the geosynthetics model, i.e., using the built-in command flow and importing the geosynthetics geometry from the third-party software. The second one was adopted to build the geocell models in this study. For importing, readers can refer to the method proposed by Gedela and Karpurapu (2021) to build honeycomb-shaped and diamond-shaped geocells. Furthermore, some vertical geocell walls extended from the geocell junctions to connect the clamp and geocells. The numerical pullout model of geocell-reinforced sand is presented in Fig. 2.

The Strain-Softening/Hardening model, instead of the Mohr-Coulomb model, was used to simulate the behavior of sand. The constitutive model allows the representation of nonlinear material softening or hardening behavior based on prescribed variations of the Mohr-Coulomb model properties (i.e., cohesion, friction, dilation, and tensile strength) as functions of the deviatoric plastic strain. It can be assumed that the total strain ($\varepsilon$) in the soil is purely elastic, i.e., $\varepsilon = \varepsilon^e$, up to the yield point and both elastic and plastic strains ($\varepsilon = \varepsilon^e + \varepsilon^p$) after the yield point. Compared to the Mohr-Coulomb model, the model can modify the shear strength parameters (cohesion, friction, and dilation) based on the accumulated plastic strain. The users can redefine these parameters as a piecewise linear function concerning the plastic shear strain in a tabular manner. Fig. 3 presents a detailed explanation of the Strain-Softening/Hardening model. Furthermore, regarding geocells, the elastic constitutive model and Mohr-Coulomb failure criterion were used to simulate the geosynthetics and the interface of soil and geosynthetics. In this study, the numerical parameters were obtained by combaining these two ways: referring to the soil properties from the literature (Fakharian and Pilban 2021) and back-calculating to make the numerical results close to the experimental data. It is worth noting that although the Young modulus was not given in the literature (Fakharian and Pilban 2021) and this study adopted 15 MPa as its value, its value does not affect the numerical pullout results. Tables 2 and 3 showdetailed used parameters of sand and geocell.

In the literature, Fakharian and Pilban (2021) used thin polyacrylic plexiglass plates to eliminate the friction

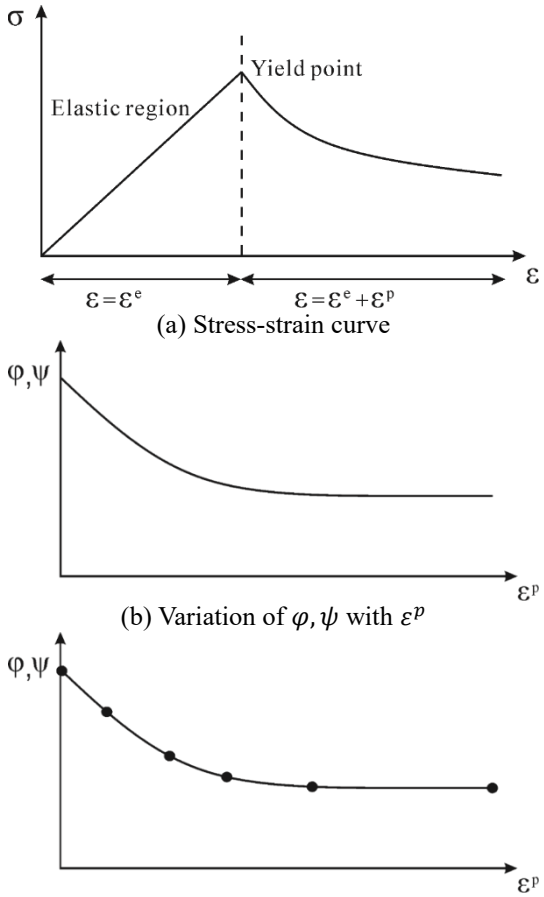


(a) Stress-strain curve

(b) Variation of $\varphi, \psi$ with $\varepsilon^p$

(c) Piecewise linear variation of $\varphi, \psi$ with $\varepsilon^p$

Fig. 3 Schematic representation of Strain-Softening/Hardening model

Table 2 Properties of soil and geocell in the validation modeling

| Parameters | Value |
|---|---|
| Sand | |
| Young modulus, $M$ (MPa) | 15 |
| Poisson's ratio, ϑ | 0.3 |
| Cohesion, $c$ (kPa) | 0.0 |
| Friction, φ (°) | See Table 3 |
| Dilation, Ψ (°) | See Table 3 |
| Density, $\rho$ (kg/m$^3$) | 1900 |
| Geocells | |
| Young modulus, $M_g$ (MPa) | 1000 |
| Poisson's ratio, ϑ | 0.45 |
| Interface shear modulus $k_i$ (MPa/m) | 2.3 |
| Interface cohesion, $c_i$ (kPa) | 0.0 |
| Interface friction, $\varphi_i$ (°) | 19.2 |
| Thickness of geocell, t (mm) | 1.5 |

between the soil and longitudinal box sides. For numerical modeling, only the normal direction of the lateral boundary was fixed to achieve it. The top boundary was set free to apply the normal stress to the model. In addition, the normal displacement of the boundary of the internal sleeve was also fixed to avoid the collapse of soils in null zones. The X-

Table 3 Variation of shear strength parameters with plastic strain

| Plastic strain, $\varepsilon^p$ (%) | Sand | |
|---|---|---|
| | Friction angle (°) | Dilation angle (°) |
| 0 | 23.5 | 0.0 |
| 0.25 | 28.0 | 0.0 |
| 0.5 | 34.0 | 4.0 |
| 0.75 | 35.5 | 5.5 |
| 1.0 | 35.8 | 5.8 |
| 2.0 | 36.0 | 6.0 |

direction movement velocity of the geocell sheets clamped at the front end was set as -2.0e-6 m/steps to simulate the pullout behavior. A series of FISH codes were programmed to capture the unbalanced force in the X direction, representing the pullout forced in tests. Incremental steps of 45000 were inputted to reach the target displacement of the clamp (frontal geocell sheets).

## 4. Results and discussions

### *4.1 Validation of numerical simulation results*

The variation of pullout force with frontal displacement (FD) is compared with the experimental results in Fig. 4. It can be seen that the FDM simulation results show a good agreement with the corresponding model test results. All data curves present the strain-hardening form. In Table 3, the friction angle and dilation angle increase with the plastic strain increase, representing that the stress-strain curve of unreinforced sand is the type of strain-hardening. Also, it is suitable for the characteristic of sand of medium density of 45%. Nevertheless, the mechanical property of sand is not a critical factor. A crucial example to prove this viewpoint is that the peak value point occurs in the pullout force vs. FD curves of geogrid-reinforced soil (Fakharian and Pilban, 2021). Also, the influenced areas and the mobilized geocell pockets are significant factors in determining whether the curves have a peak point.

### *4.2 The horizontal displacement of infilled sand and geocells*

Han *et al.* (2013), Fakharian and Pilban (2021) analyzed the mechanism of geocell resisting the pullout behavior based on the experimental results. These presented explanations only account for their studies; further, the mechanism needs more intuitive results to prove it. In this section, the contours of horizontal displacement of infilled sand (see Fig. 5) and geocells (see Fig. 6) with the increase of FD under the normal stress of 23 kPa are shown to perfect and verify the mechanism. The integral pullout process is divided into six stages according to the 15 mm interval of FD. All contours and data are extracted at the plane of elevation of 250 mm, which is the middle plane of

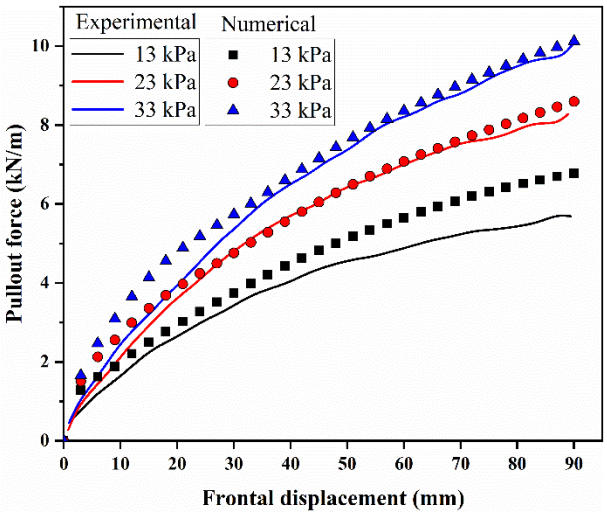


Fig. 4 The variation of pullout force with the frontal displacement of geocell reinforcement

the numerical model. Due to the similar results of various normal stress, the contours corresponding to other results are not presented in this study.

In FLAC$^{3D}$, the normal stiffness modulus between geogrid elements and contacted soil is set to infinity by default. Hence, the two synergistically deformed in the area of element nodes. From Figs. 5 and 6, geocells' pullout behavior presents progressive development instead of all cell pockets being mobilized to resist the pullout force. For the initial stage (see Fig. 5 (a) and Fig. 6), large deformation occurs in the soil locating the frontal side, and about one-third of cell pockets and sand along the X direction are driven, indicating that only a small number of cells contribute to the pullout resistance. The contours show the form of sunken. With the increase in FD, in Figs. 5(b)-5(f) and Fig. 6, only a few geocells continue to be mobilized, which take up about one-half of geocells at most. Although the contour of 1 mm is almost parallel to the boundary, all contours greater than 2 mm also present a sunken form. It indicates that geocells are not deformed side by side in the pullout behavior. The geocells in the middle part are less deformed due to the interaction of the honeycomb structure, while the geocells on both sides are subjected to less interaction and deform more. Moreover, all contours in Fig. 5 and the data in Fig. 6 show that the increased influenced area does not change much; however, the horizontal displacement of mobilized geocells and infilled sand increases proportionally. Due to the vertical walls and honeycomb-shaped cells, very few pullout forces can be transferred to the end of the embedded geocells. The geocells in the influenced area carry the main pullout force and undergo large deformation.

### *4.3 Passive resistance transmission*

The pullout resistance is composed of two: the shear resistance developed at the interface between the geocell-reinforced layer and unreinforced soil and the anchorage resistance induced by the passive pressure in the geocell pockets (Fakharian and Pilban 2021, Isik and Gurbuz 2020,

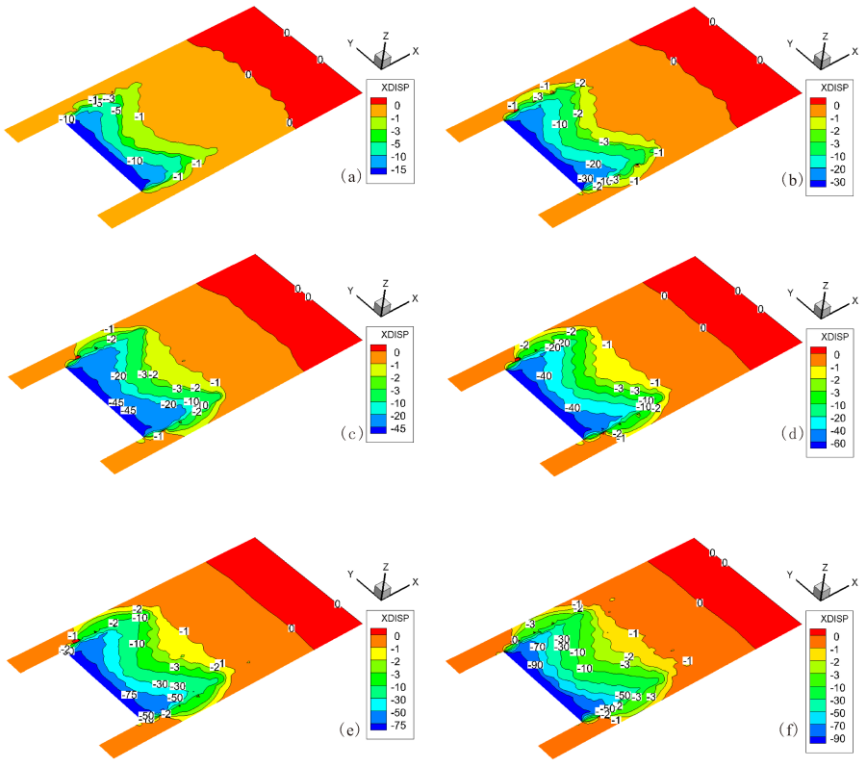


Fig. 5 Contours of X-direction deformation of sandy soil in the middle of geocell reinforced layer: (a) FD of 15 mm, (b) FD of 30 mm, (c) FD of 45 mm, (d) FD of 60 mm, (e) FD of 75 mm and (f) FD of 90 mm

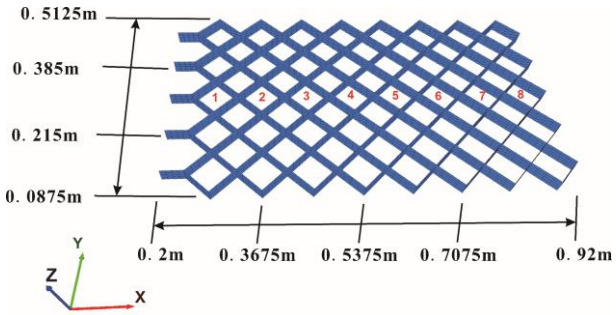


(a) The coordinate of geocells in the numerical model

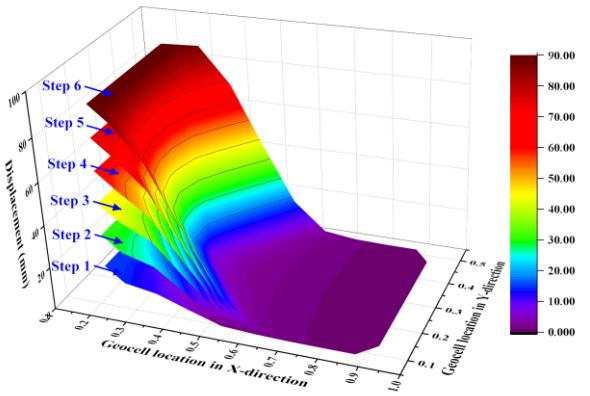


(b) X-direction displacement of geocell nodes

Fig. 6 The X-direction displacement of geocells nodes during the pullout process

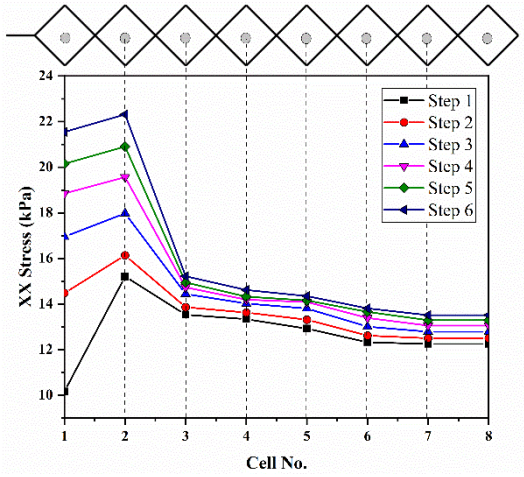


Fig. 7 Response of lateral pressure during the pullout process

Isik *et al.* 2022). The interface resistance is the main contributor of pullout resistance to the two-dimensional geosynthetics (geogrids and geotextiles), while passive resistance induced by vertical walls is it for geocells. Hence, in this section, the variation of passive pressure, represented by XX stress, with geocells location under the normal stress 23 kPa is illustrated in Fig. 7. Geocells are divided into eight columns along the length direction, as shown in Fig. 6, in which each column includes five geocell pockets. The xx pressure of the center position of each pocket was monitored in the numerical analysis. Plus, the average values of five pockets were determined to represent the passive resistance of geocells in each column.

From Fig. 7, the average XX stress of the geocells in the first column is less than the value of the second column, where the frontal sand was not restricted, causing it.

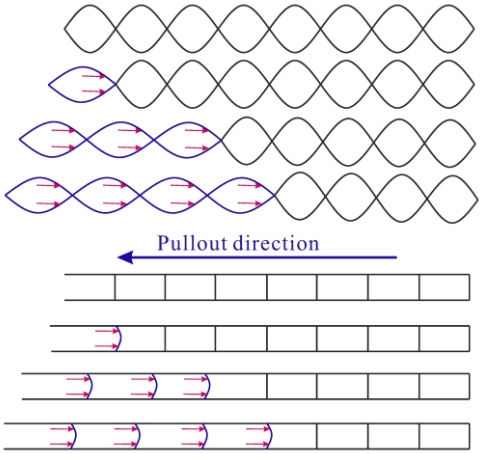


Fig. 8 Deformation patterns of diamond-shaped geocells (modified from Han *et al.* (2013))

Perhaps much sand was squeezed out in the sleeve during the pullout tests. In addition, geocells in the one to four columns are mobilized with the pullout process, which is similar to the law shown in section 4.2. The passive resistance of geocells decreases dramatically starting in the third column, indicating that the geocells in the front of the fourth column are the main contributor to the pullout resistance. The mechanism of load transmission and deformation patterns in Fig. 8 can account for the pullout behavior. The geocells in the first column start to deform and provide the pullout resistance, and until the geocells in the first column reach the residual state, the geocells in the second and third columns deform and provide resistance. This response to pullout behavior can be defined as the pattern of progressive deformation.

## 5. Factors affecting the pullout force of geocell reinforcement

This section discusses the effect of various geocell properties and pullout displacement, which could affect the pullout behavior of geocell reinforced sand, with the help of the validated numerical model. The key parameters are studied, including geocell modulus, aspect ratio, interface friction, reinforced length, and pullout displacement.

According to the baseline model illustrated in Fig. 2, Table 2, and Table 3, the modulus of the geocell was changed from 500 MPa to 4.0 Gpa. The variation of pullout force with geocell modulus under different normal stress and FD are plotted in Fig. 9(a). The pullout force increases with the increase of geocell modulus; however, the slope of curves decreases gradually. As the geocell modulus increases, the higher confining pressure and passive pressure will be exerted on the infilled soil under the same FD, which benefits to increase in the pullout force.

In this study, the diameter of cell pockets was changed to represent different aspect ratios (geocell height/diameter of cell pockets). As mentioned in Section 3, Fig. 2 and Fig. 6, the dimensions of the geocell specimens are 425 mm in width and 720 mm in length. There are five cell pockets along the width direction. Hence, in this study, the width of the geocell layer is constant, and the number of cell pockets in the width direction is changed to three, five, eight, eleven, and fourteen. The corresponding aspect ratios are 0.22, 037, 0.59, 0.81, and 1.03, respectively. Fig. 9(b) shows the variation of pullout force with the aspect ratio of geocells. It can be concluded that the pullout force increases linearly as the aspect ratio increases. The geocells with a small aspect ratio can provide more confining and passive pressure to resist the pullout behavior.

Many manufacturing techniques, such as embossing or perforating, could add surface roughness, which supplies more friction between soil and geocells. In this section, the interface friction is changed to investigate its influence on the pullout force. In the baseline model, the interface friction is estimated by multiplying the tangent of the friction angle with a discount factor of 0.8. Hence, different interface friction values are selected as 0.5, 0.6, 0.7, 0.8, and 0.9 in this section, as shown in Fig. 9(c). It is observed that the interface friction affects the pullout force little. The pullout force shows little change with the increase in interface friction, suggesting that the friction between soil and geocell is not the main contributor, and the passive force is. Users can not level up the pullout resistance by improving the roughness of the geocell surface.

Sections 4.2 and 4.3 show that, for the baseline model, all geocell pockets are not mobilized even FD to 90 mm. The embedded length and FD significantly influence the pullout force. As shown in Fig. 9(d), the pullout force almost remains constant in subsequent when the embedded length is up to about 0.38 m. This conclusion corresponds to the law in sections 4.2 and 4.3. Even if the FD is 90 mm, the influenced area accounts for about half of the geocell mattress along the length direction. In addition, although the FD is up to 270 mm, as illustrated in Fig. 9(e), three times the FD of the baseline model, there is no peak value in the curve of pullout force vs. FD. It indicates that the pullout load has not transferred to the end of the geocell. Different from the two-dimensional geosynthetics, the vertical walls can provide more passive pressure, which benefits to improve the pullout resistance but hind the load transmission

## 6. Sensitivity analysis and predicted model

### *6.1 Sensitivity analysis based on the orthogonal design*

Section 5 discusses some parameters and their influence on pullout behavior. The degree of influence can not be determined. Hence, the orthogonal design was used in this section to order the parameters to provide some references to choose the optimum geocells. Four parameters were considered, i.e., geocell modulus, aspect ratio, a discount factor of interface friction (DFIF), and embedded length. Each parameter includes three levels. Therefore, the orthogonal table L18.3.6 (see Table 4) is used for analysis, where the pullout force at FD of 90 mm under the normal pressure of 23 kPa is as the evaluation index ($y_i$), The result of the extreme difference analysis is also listed in this Table.

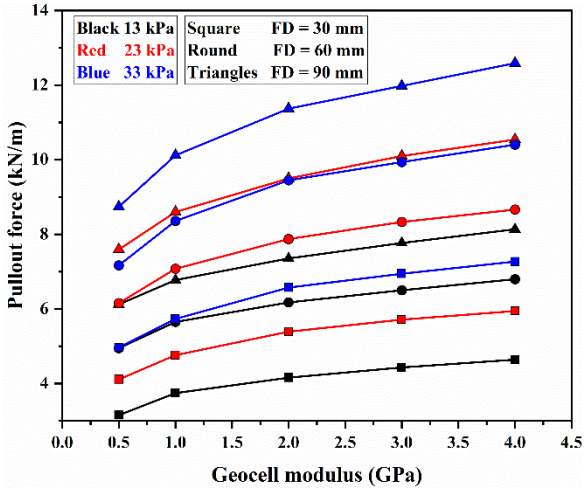


(a) Different geocell modulus

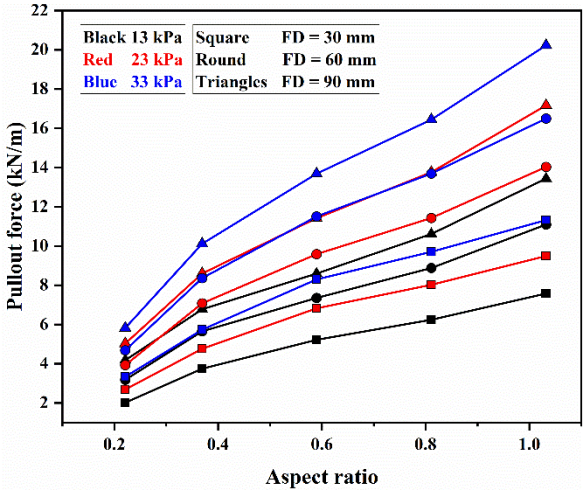


(b) Different aspect ratio

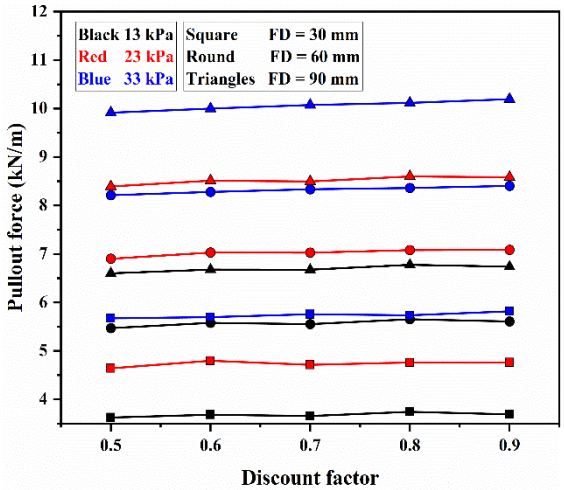


(c) Different discount factors of interface

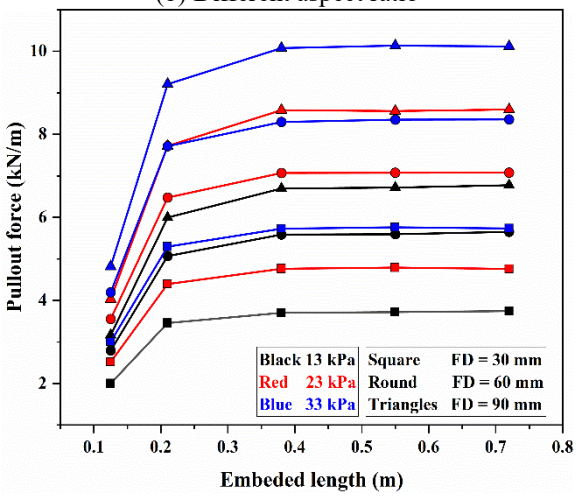


(d) Different embedded lengths of geocell

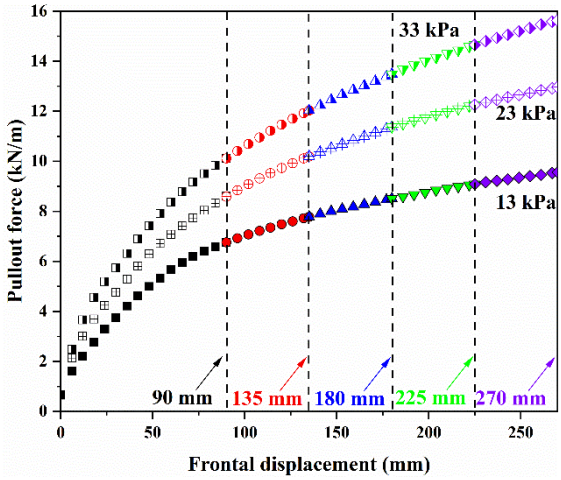


(e) Different frontal displacement

Fig. 9 Pullout force VS frontal displacement curves

$y_{mn}$ is the sum of the $y_i$ corresponding to the n level of the m parameter. $\overline{y_{mn}}$ is the average value of $y_{mn}$. Moreover, $R_j$ is the difference value of $\max[\overline{y_{j1}}, \overline{y_{j2}}, \overline{y_{j3}}]$ and $\min[\overline{y_{j1}}, \overline{y_{j2}}, \overline{y_{j3}}]$. Based on this value, the weights of the four influencing factors are ranked as embedded length, aspect ratio, geocell modulus, and interface friction.

### *6.2 Predicted model*

The aspect ratio ($R$), geocell modulus ($M$), embedded length ($L$), frontal displacement ($D$), and normal stress ($N$) are taken into consideration to develop a predicted model. In practice, there is no specific factor to represent the

Table 4 Orthogonal Table L18.3.6

| No. | Geocell modulus (GPa) | Aspect ratio | DFIF | embedded length | | | $y_i$ |
|---|---|---|---|---|---|---|---|
| 1 | 0.5 | 0.37 | 0.6 | 0.125 | 1 | 1 | 3.61 |
| 2 | 0.5 | 0.37 | 0.7 | 0.21 | 3 | 3 | 6.78 |
| 3 | 0.5 | 0.59 | 0.6 | 0.38 | 3 | 2 | 10.12 |
| 4 | 0.5 | 0.59 | 0.8 | 0.125 | 2 | 3 | 4.95 |
| 5 | 0.5 | 0.81 | 0.7 | 0.38 | 2 | 1 | 11.90 |
| 6 | 0.5 | 0.81 | 0.8 | 0.21 | 1 | 2 | 10.40 |
| 7 | 1 | 0.37 | 0.6 | 0.38 | 2 | 3 | 8.46 |
| 8 | 1 | 0.37 | 0.8 | 0.125 | 3 | 2 | 4.03 |
| 9 | 1 | 0.59 | 0.7 | 0.21 | 2 | 2 | 9.51 |
| 10 | 1 | 0.59 | 0.8 | 0.38 | 1 | 1 | 11.19 |
| 11 | 1 | 0.81 | 0.6 | 0.21 | 3 | 1 | 10.84 |
| 12 | 1 | 0.81 | 0.7 | 0.125 | 1 | 3 | 6.27 |
| 13 | 2 | 0.37 | 0.7 | 0.38 | 1 | 2 | 9.43 |
| 14 | 2 | 0.37 | 0.8 | 0.21 | 2 | 1 | 8.40 |
| 15 | 2 | 0.59 | 0.6 | 0.21 | 1 | 3 | 9.94 |
| 16 | 2 | 0.59 | 0.7 | 0.125 | 3 | 1 | 5.22 |
| 17 | 2 | 0.81 | 0.6 | 0.125 | 2 | 2 | 6.39 |
| 18 | 2 | 0.81 | 0.8 | 0.38 | 3 | 3 | 15.60 |
| $y_{j1}$ | 47.76 | 40.71 | 49.36 | 30.47 | 50.84 | 51.16 | |
| $y_{j2}$ | 50.30 | 50.92 | 49.11 | 55.87 | 49.61 | 49.88 | |
| $y_{j3}$ | 54.98 | 61.40 | 54.56 | 66.69 | 52.59 | 52.00 | |
| $\overline{y_{j1}}$ | 7.96 | 6.78 | 8.23 | 5.08 | 8.47 | 8.53 | |
| $\overline{y_{j2}}$ | 8.38 | 8.49 | 8.19 | 9.31 | 8.27 | 8.31 | |
| $\overline{y_{j3}}$ | 9.16 | 10.23 | 9.09 | 11.12 | 8.76 | 8.67 | |
| $R_j$ | 1.20 | 3.45 | 0.91 | 6.04 | 0.50 | 0.35 | |

surface roughness. Also, the above analysis proves that it little influences the pullout force ($F$). Hence, this parameter is not included in this model. The predicted equation can be expressed simply as

$$F = f(R, M, L, D, N) \tag{1}$$

According to the data from Fig. 9, the following predicted equation between the dependent and independent variables is proposed to predict the pullout force. Compared with the other predicted models, it shows a significant relationship between independent and dependent variables and reflects the extent to which multiple independent variables affect a dependent variable. In addition, the regression equation is simple, making it easy to generalize.

$$\left[M^{\alpha} + R^{\beta} + L^{\theta} + Lg(D)\right] * N^{\omega} = F$$

Where $R$, $M$, $L$, $D$, and $N$ are the independents as the unit of dimensionless, GPa, m, m, and kPa, respectively. $F$ is the dependent variable as the unit of kN/m. $\alpha, \beta, \theta$, and $\omega$ are the dimensionless constants. The values of these constants obtained through multiple regression analyses are as follows:

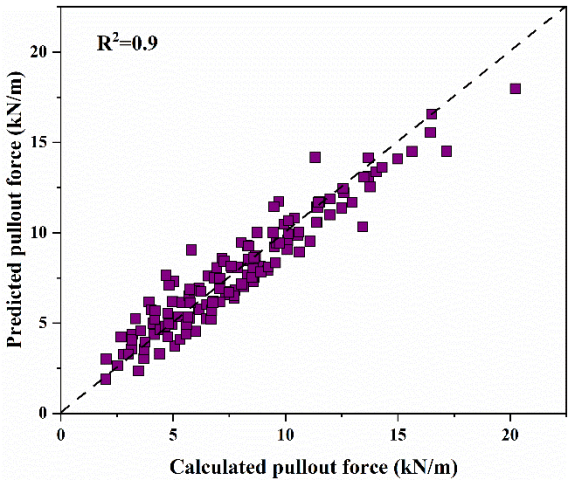


Fig. 10 Comparison results between the predicted values and data of parametric studies

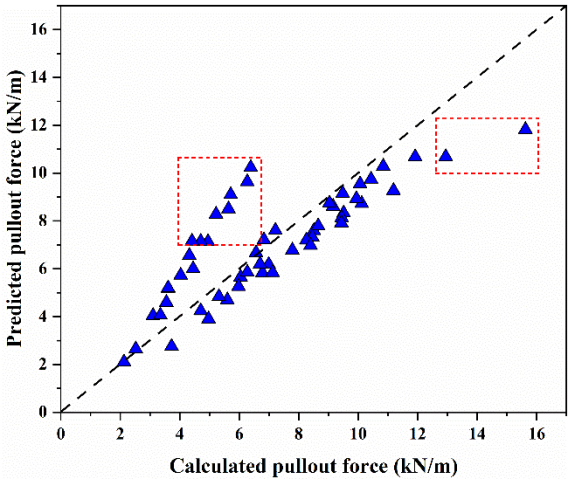


Fig. 11 Comparison results between the predicted values and data of orthogonal design

$$\alpha = 0.12756, \beta = 1.37754, \theta = 0.41211, \omega = 0.59444$$

The coefficient of correlation between the predicted and calculation values of F is found to be 0.90, as illustrated in Fig. 10, which indicates that the proposed regression equation can predict the pullout force of geocell-reinforced sand. Moreover, the data in Fig. 9 results from the single-factor analysis, which can not represent all reinforced cases. The orthogonal analysis, shown in section 6.1, only uses limited cases to represent almost all cases. Hence, the data in section 6.1 is also used to validate the proposed model, which can check the model's suitability for all reinforced cases. Although only the pullout force at the FD of 90 mm is listed in Table 4, the values at the FD of 30 mm, 60 mm, and 90 mm are used to verify this model. Fig. 11 illustrates the comparison between numerical results and predicted results. Some points inside the red box can not be predicted accurately. The authors check this point carefully and find that these points almost belong to the case where the aspect ratio is 0.81 and the embedded length is 0.125 simultaneously. To take the opinions above, the proposed model can predict the pullout force of geocell reinforcement

well. However, due to the diamond-shaped geocell being used in this study, the suitability of honeycomb-shaped geocells still needs a deep study to validate.

## 7. Conclusions

In this paper, after validating against the model test results, the pullout behavior evolution of geocell reinforcement was investigated through numerical technologies. Some contours and curves benefit readers in understanding the mechanism and load transfer path deeply. Further, parametric studies and sensitivity analyses were conducted to explore the tendency and degree of influence.

A regression model was proposed to predict the pullout force, where the comparison data validate the prediction accuracy. The conclusions and limitations of this study can be drawn as follows:

a) The Strain-Softening/Hardening model, where users could define the variation of friction and dilation with the plastic strain, was used to simulate the behavior of medium-density sand. Moreover, a series of FISH codes were programmed to capture the unbalanced force of nodes in the X direction, representing the pullout force. The comparison results illustrate that the numerical model can well simulate the pullout behavior of geocell reinforcement.

b) The response to the pullout behavior of geocell reinforcement can be defined as the pattern of progressive deformation. The results of horizontal displacement of infill sand and geocell nodes and passive resistance transmission prove that the geocell pockets are mobilized gradually to resist the pullout force. Hence, the main contributor is the passive resistance of vertical walls, not the interface resistance between the geocell-reinforced and unreinforced layers. Even if the FD is 90 mm, the pullout load has not transferred to the end of the geocell layer. About half of the geocell pockets are mobilized in this case.

c) Except for the interface roughness of the geocell, the geocell modulus, aspect ratio, embedded length, and FD are beneficial to the pullout resistance of geocell reinforcement. In addition, the weights of influencing factors are ranked as embedded length, aspect ratio, geocell modulus, and interface friction.

d) A regression model was proposed in this study to predict the pullout load of geocell reinforcement. The aspect ratio, geocell modulus, embedded length, frontal displacement, and normal stress are considered in this model. Users can determine the pullout force based on these parameters. Some comparisons were concluded and showed the accuracy of the predicted model.

## Acknowledgments

This work was supported by the National Natural Science Foundation of China (Nos. 420772622, 42077261, and 41972294). In addition, Yang Zhao wants to thank Juan Li and Guan-lin Zhao for their encouragement and support over the past few years.

## References

Altay, G., Kayadelen, C., Canakci, H., Bagriacik, B., Ok, B. and Oguzhanoglu, M.A. (2021), "Experimental investigation of deformation behavior of geocell retaining walls", *Geomech. Eng.*, **27**(5), 419-431. https://doi.org/10.12989/gae.2021.27.5.419.

Ardakani, A. and Namaei, A. (2021), "Numerical investigation of geocell reinforced slopes behavior by considering geocell geometry effect", *Geomech. Eng.*, **24**(6), 589-597. https://doi.org/10.12989/gae.2021.24.6.589.

Bathurst, R.J. and Karpurapu, R. (1993), "Large-scale triaxial compression testing of geocell-reinforced granular soils", *Geotech. Test. J.*, **16**(3), 296-303. https://doi.org/10.1520/GTJ10050J.

Biswas, S. and Mittal, S. (2017), "Square footing on geocell reinforced cohesionless soils", *Geomech. Eng.*, **13**(4), 641-651. https://doi.org/10.12989/gae.2017.13.4.641.

Derksen, J., Ziegler, M. and Fuentes, R. (2021), "Geogrid-soil interaction: A new conceptual model and testing apparatus", *Geotext. Geomembranes*, **49**(5), 1393-1406. https://doi.org/10.1016/j.geotexmem.2021.05.011.

Fakharian, K. and Pilban, A. (2021), "Pullout tests on diagonally enhanced geocells embedded in sand to improve load-deformation response subjected to significant planar tensile loads", *Geotext. Geomembranes*, **49**(5), 1229-1244. https://doi.org/10.1016/j.geotexmem.2021.04.002.

Gedela, R. and Karpurapu, R. (2021), "Influence of pocket shape on numerical response of geocell reinforced foundation systems", *Geosynth. Int.*, **28**(3), 327-337. https://doi.org/10.1680/jgein.20.00042.

Girout, R., Blanc, M., Thorel, L. and Dias, D. (2018), "Geosynthetic reinforcement of pile-supported embankments", *Geosynth. Int.*, **25**(1), 37-49. https://doi.org/10.1680/jgein.17.00032.

Halder, K. and Chakraborty, D. (2020), "Influence of soil spatial variability on the response of strip footing on geocell-reinforced slope", *Comput. Geotech.*, **122**, 103533. (https://doi.org/10.1016/j.compgeo.2020.103533.

Han, X.Y., Kiyota, T. and Tatsuoka, F. (2013), "Interaction mechanism between geocell reinforcement and gravelly soil by pullout tests", *Bull. Earth Resistance Struct.*, **46**, 53-62.

Isik, A., Anil, O. and Gurbuz, A. (2022), "Proposed novel bond-slip model for geocell reinforcement under pull-out loading condition", *Geotechnique*, **73**(11), 1-44. https://doi.org/10.1680/jgeot.21.00120.

Isik, A. and Gurbuz, A. (2020), "Pullout behavior of geocell reinforcement in cohesionless soils", *Geotext. Geomembranes*, **48**(1), 71-81. https://doi.org/10.1016/j.geotexmem.2019.103506.

Karnamprabhakara, B.K. and Balunaini, U. (2021), "Modified axial pullout resistance factors of geogrids embedded in pond ash", *Geotext. Geomembranes*, **49**(5), 1245-1255. https://doi.org/10.1016/j.geotexmem.2021.04.003.

Khalaj, O., Tafreshi, S.N.M., Mask, B. and Dawson, A.R. (2015), "Improvement of pavement foundation response with multi-layers of geocell reinforcement: Cyclic plate load test", *Geomech. Eng.*, **9**(3), 373-395. https://doi.org/10.12989/gae.2015.9.3.373.

Khedkar, M.S. and Mandal, J.N. (2009), "Pullout behaviour of cellular reinforcements", *Geotext. Geomembranes*, **27**(4), 262-271. https://doi.org/10.1016/j.geotexmem.2008.12.003.

Khorsandiardebili, N. and Ghazavi, M. (2021), "Static stability analysis of geocell-reinforced slopes", *Geotext. Geomembranes*, **49**(3), 852-863. https://doi.org/10.1016/j.geotexmem.2020.12.012.

Kumar, A., Singh, A.P. and Chatterjee, K. (2019), "Ground

improvement using geocells to enhance trafficability in desert soils", *Geomech. Eng.*, **19**(1), 71-78. https://doi.org/10.12989/gae.2019.19.1.071.

Latha, G.M. (2011), "Design of geocell reinforcement for supporting embankments on soft ground", *Geomech. Eng.*, **3**(2), 117-130. https://doi.org/10.12989/gae.2011.3.2.117.

Lu, W., Miao, L., Wang, E., Zhang, J., Zhang, Y. and Wang, H. (2020), "A case study on geogrid-reinforced and pile-supported widened highway embankment", *Geosynth. Int.*, **27**(3), 261-274. https://doi.org/10.1680/jgein.19.00024.

Luo, X.W., Lu, Z., Yao, H.L., Zhang, J.B. and Song, W. (2021), "Experimental study on soft rock subgrade reinforced with geocell", *Road Mater. Pavement Des.*, **23**(9), 1-15. https://doi.org/10.1080/14680629.2021.1948907.

Luo, X.W., Lu, Z., Zhang, J.B. and Yao, H.L. (2023), "Study on performance of geocell-reinforced red clay subgrade", *Geosynth. Int.*, 1-41. https://doi.org/10.1680/jgein.23.00068.

Mirzaeifar, H., Hatami, K. and Abdi, M.R. (2022), "Pullout testing and Particle Image Velocimetry (PIV) analysis of geogrid reinforcement embedded in granular drainage layers", *Geotext. Geomembranes*, **50**(6), 1083-1109. https://doi.org/10.1016/j.geotexmem.2022.06.008.

Moraci, N. and Recalcati, P. (2006), "Factors affecting the pullout behaviour of extruded geogrids embedded in a compacted granular soil", *Geotext. Geomembranes*, **24**(4), 220-242. https://doi.org/10.1016/j.geotexmem.2006.03.001.

Mosallanezhad, M., Taghavi, S.H.S., Hataf, N. and Alfaro, M.C. (2016), "Experimental and numerical studies of the performance of the new reinforcement system under pull-out conditions", *Geotext. Geomembranes*, **44**(1), 70-80. https://doi.org/10.1016/j.geotexmem.2015.07.006.

Mukherjee, S., Kumar, L., Choudhary, A.K. and Babu, G.L.S. (2021), "Pullout resistance of inclined anchors embedded in geogrid reinforced sand", *Geotext. Geomembranes*, **49**(5), 1368-1379. https://doi.org/10.1016/j.geotexmem.2021.05.009.

Namaei-kohal, A., Ardakani, A. and Hassanlourad, M. (2022), "Hypoplastic soil model parameters calibration for Tehran silica sand and verification with a monotonic geocell pullout test", *Arabian J. Geosci.*, **15**(9), 824. https://doi.org/10.1007/s12517-022-10110-9.

Pant, A. and Ramana, G.V. (2022), "Prediction of pullout interaction coefficient of geogrids by extreme gradient boosting model", *Geotext. Geomembranes*, **50**(6), 1188-1198. https://doi.org/10.1016/j.geotexmem.2022.08.003.

Ren, F., Huang, Q., Liu, Q. and Wang, G. (2022), "Numerical study on the pull-out behaviour of planar reinforcements with consideration of residual interfacial shear strength", *Transp. Geotech.*, **35**, 100766. https://doi.org/10.1016/j.trgeo.2022.100766.

Saikia, R. and Dash, S.K. (2024), "Load carrying mechanism of geocell reinforced embankment on soft soil", *Transp. Res. Rec.*, 03611981241230317. https://doi.org/10.1177/03611981241230317.

Saride, S., Pradhan, S., Sitharam, T.G. and Puppala, A.J. (2013), "Numerical analysis of geocell reinforced ballast overlying soft clay subgrade", *Geomech. Eng.*, **5**(3), 263-281. https://doi.org/10.12989/gae.2013.5.3.263.

Tafreshi, S.N.M., Darabi, N.J. and Dawson, A.R. (2018), "Cyclic loading response of footing on multilayered rubber-soil mixtures", *Geomech. Eng.*, **14**(2), 115-129. https://doi.org/10.12989/gae.2018.14.2.115.

Wang, Z., Jacobs, F. and Ziegler, M. (2016), "Experimental and DEM investigation of geogrid–soil interaction under pullout loads", *Geotext. Geomembranes*, **44**(3), 230-246. https://doi.org/10.1016/j.geotexmem.2015.11.001.

Wijerathna, M. and Liyanapathirana, D.S. (2020), "Load transfer mechanism in geosynthetic reinforced column-supported embankments", *Geosynth. Int.*, **27**(3), 236-248. https://doi.org/10.1680/jgein.19.00022.

Yang, X.M., Han, J., Leshchinsky, D. and Parsons, R.L. (2013), "A three-dimensional mechanistic-empirical model for geocell-reinforced unpaved roads", *Acta Geotech.*, **8**(2), 201-213. https://doi.org/10.1007/s11440-012-0183-6.

Yang, X.M., Han, J., Pokharel, S.K., Manandhar, C., Parsons, R.L., Leshchinsky, D. and Halahmi, L. (2012), "Accelerated pavement testing of unpaved roads with geocell-reinforced sand bases", *Geotext. Geomembranes*, **32**(95-103. https://doi.org/10.1016/j.geotexmem.2011.10.004.

Zhao, Y., Lu, Z., Liu, J., Ye, L., Xu, W.Z. and Yao, H.L. (2023), "Effect of cohesion of infill materials on the performance of geocell-reinforced cohesive soil subgrade", *Geomech. Eng.*, **33**(3), 301-315. https://doi.org/10.12989/gae.2023.33.3.301.

Zhao, Y., Lu, Z., Liu, J. and Yao, H.L. (2024a), "Numerical study on shear behavior of geocell-reinforced layer based on large-scale direct shear tests", *KSCE J. Civ. Eng.*, **28**(7), 2613-2624. https://doi.org/10.1007/s12205-024-2458-5.

Zhao, Y., Lu, Z., Yao, H.L., Ye, L., Cheng, M., Tang, C.X., Qiu, Y. and Yuan, X.Z. (2024b), "A regression model for predicting the subgrade modulus of geocell-reinforced sand beds", *Int. J. Geomech.*, **24**(1), 06023022. https://doi.org/doi:10.1061/IJGNAI.GMENG-7378.

*CC*